Design trade-off and proof of concept for LOUPE, the Lunar Observatory for Unresolved Polarimetry of Earth

Hoeijmakers, H. J.; Arts, M. L J; Snik, F.; Keller, C. U.; Kuiper, J. M.

DOI
10.1364/OE.24.021435

Publication date
2016

Document Version
Final published version

Published in
Optics Express

Research Article | Vol. 24, No. 19 | 19 Sep 2016 | OPTICS EXPRESS 21435

Optics EXPRESS

Design trade-off and proof of concept for LOUPE, the Lunar Observatory for Unresolved Polarimetry of Earth

H. J. HOEIJMAKERS,[1,*] M. L. J. ARTS,[2] F. SNIK,[1] C. U. KELLER,[1] AND J. M. KUIPER[3]

[1]*Leiden Observatory, Leiden University, Niels Bohrweg 2, 2333 CA Leiden, The Netherlands*
[2]*ESTEC, Keplerlaan 1, 2200 AG Noordwijk, The Netherlands*
[3]*Faculty of Aerospace Engineering, Delft Technical University, Kluyverweg 1, 2629 HA Delft, The Netherlands*
[*]*hoeijmakers@strw.leidenuniv.nl*

Abstract: We provide a proof of the technical feasibility of LOUPE, the first integral-field snapshot spectropolarimeter, designed to monitor the reflected flux and polarization spectrum of Earth. These are to be used as benchmark data for the retrieval of biomarkers and atmospheric and surface characteristics from future direct observations of exoplanets. We perform a design trade-off for an implementation in which LOUPE performs snapshot integral-field spectropolarimetry at visible wavelengths. We used off-the-shelf optics to construct a polarization modulator, in which polarization information is encoded into the spectrum as a wavelength-dependent modulation, while spatial resolution is maintained using a micro-lens array. The performance of this design concept is validated in a laboratory setup. Our proof-of-concept is capable of measuring a grid of 50 × 50 polarization spectra between 610 and 780 nm of a mock target planet - proving the merit of this design. The measurements are affected by systematic noise on the percent level, and we discuss how to mitigate this in future iterations. We conclude that LOUPE can be small and robust while meeting the science goals of this particular space application, and note the many potential applications that may benefit from our concept for doing snapshot integral-field spectropolarimetry.

OCIS codes: (110.0280) Remote sensing and sensors; (110.5405) Polarimetric imaging; (120.5410) Polarimetry; (120.6200) Spectrometers and spectroscopic instrumentation; (290.5855) Scattering, polarization; (300.6550) Spectroscopy, visible; (350.1260) Astronomical optics; (350.1270) Astronomy and astrophysics.

References and links

1. N. Hagen and M. W. Kudenov, "Review of snapshot spectral imaging technologies," Opt. Eng. **52**, 090901 (2013).
2. E. L. Dereniak, "Infrared spectro-polarimeter," Proc. SPIE **5957** 202–211 (2005).
3. M. W. Kudenov, M. E. L Jungwirth, E. L. Dereniak and G. R. Gerhart "White light Sagnac interferometer for snapshot linear polarimetric imaging," Opt. Express **17**, 22520–22534 (2009)
4. M. W. Kudenov, M. J. Escuti, E. L. Dereniak and K. Oka "White-light channeled imaging polarimeter using broadband polarization gratings," Appl. Opt. **50**, 2283–2293 (2011)
5. M. W. Kudenov and E. L. Dereniak "Compact real-time birefringent imaging spectrometer," Opt. Express **20**, 17973–17986 (2012).
6. K. Oka and T. Kato, "Spectroscopic polarimetry with a channeled spectrum," Opt. Lett. **24**, 1475–1477 (1999).
7. F. Snik, T. Karalidi, and C. U. Keller, "Spectral modulation for full linear polarimetry," Appl. Opt. **48**, 1337–1346 (2009).
8. J. Tinbergen *Astronomical Polarimetry* (Cambridge University Press, 1996).
9. J. Hough, "Polarimetry: a powerful diagnostic tool in astronomy," Astron. Geophys. **47**, 3.31–3.35 (2006).
10. F. Snik and C. U. Keller, "Astronomical polarimetry: polarized views of stars and planets" in *Planets, Stars and Stellar Systems: Volume 2: Astronomical Techniques, Software and Data* Howard E. Bond Ed. (Springer Netherlands, 2013).
11. D. M. Stam, J. W. Hovenier, and L. B. F. M. Waters, "Using polarimetry to detect and characterize Jupiter-like extrasolar planets," A&A **428**, 663–672 (2004).
12. T. Karalidi, D. M. Stam, and J. W. Hovenier, "Looking for the rainbow on exoplanets covered by liquid and icy water clouds," A&A **548**, A90 (2012).
13. J. E. Hansen and J. W. Hovenier, "Interpretation of the polarization of Venus," J. Atmos. Sci. **31**, 1137–1160 (1974).

#261339 http://dx.doi.org/10.1364/OE.24.021435
Journal © 2016 Received 25 Apr 2016; revised 6 Jul 2016; accepted 13 Jul 2016; published 7 Sep 2016

Optics EXPRESS

14. M. I. Mishchenko, B. Cairns, G. Kopp, C. F. Schueler, B. A. Fafaul, J. E. Hansen, R. J. Hooker, T. Itchkawich, H. B. Maring, and L. D. Travis, "Accurate monitoring of terrestrial aerosols and total solar irradiance: introducing the Glory mission," Bull. Am. Meteorol. Soc. **88**, 677 (2007).
15. E. Duursma and M. Boisson, "Global oceanic and atmospheric oxygen stability considered in relation to the carbon cycle and to different time scales," Oceanol. Acta **17**, 117–141 (1994).
16. N. Narita, T. Enomoto, S. Masaoka, and N. Kusakabe, "Titania may produce abiotic oxygen atmospheres on habitable exoplanets," Sci. Rep. **5**, 13977 (2015).
17. S. Seager, E. L. Turner, J. Schafer, and E. B. Ford, "Vegetation's red edge: a possible spectroscopic biosignature of extraterrestrial plants," Astrobiology **5**, 372–390 (2005).
18. D. Briot, L. Arnold, S. Jacquemoud, and J. Schneider, "Present and future detection of terrestrial biomarkers on earthshine," in proceedings of IAU Symposium **293**, 65–67 (2014).
19. W. Sparks, J. Hough, L. Kolokolova, T. Germer, F. Chen, S. DasSarma, P. DasSarma, F. Robb, N. Manset, I. Reid, F. Macchetto, and W. Martin, "Circular polarization in scattered light as a possible biomarker," J. Quant. Spectrosc. Radiat. Transfer **110**, 1771–1779 (2009).
20. J. D. Carroll, "A new definition of life," Chirality **21**, 354–358 (2009).
21. D. M. Stam, "Spectropolarimetric signatures of Earth-like extrasolar planets," A&A **482**, 989–1007 (2008).
22. E. Pallé, "Earthshine observations of an inhabited planet," EAS Publication Series **41**, 505–516 (2010).
23. M. F. Sterzik, S. Bagnulo, and E. Palle, "Biosignatures as revealed by spectropolarimetry of earthshine," Nature **483**, 64–66 (2012).
24. A. Bazzon, H. M. Schmid, and D. Gisler, "Measurement of the earthshine polarization in the B, V, R, and I band as function of phase," A&A **556**, A117 (2013).
25. F. Parol, J. C. Buriez, C. Vanbauce, J. Riedi, L. C. Labonnote, M. Doutriaux-Boucher, M. Vesperini, G. Sèze, P. Couvert, M. Viollier, and F. M. Bréon, "Review of capabilities of multi-angle and polarization cloud measurements from POLDER," Adv. Space Res. **33**, 1080–1088 (2004).
26. D. Tanré, F. M. Bréon, J. L. Deuzé, O. Dubovik, F. Ducos, P. François, P. Goloub, M. Herman, A. Lifermann, and F. Waquet, "Remote sensing of aerosols by using polarized, directional and spectral measurements within the a-train: the parasol mission," Atmos. Meas. Tech. **4**, 1383–1395 (2011).
27. E. Pallé and P. R. Goode, "The Lunar Terrestrial Observatory: observing the Earth using photometers on the Moon's surface," Adv. Space Res. **43**, 1083–1089 (2009).
28. T. Karalidi, D. M. Stam, F. Snik, S. Bagnulo, W. B. Sparks, and C. U. Keller, "Observing the Earth as an exoplanet with LOUPE, the lunar observatory for unresolved polarimetry of Earth," Planet. Space Sci. **74**, 202–207 (2012).
29. S. Jones, F. Iannarilli, and P. Kebabian, "Realization of quantitative-grade fieldable snapshot imaging spectropolarimeter," Opt. Express **12**, 6559–6573 (2004).
30. F. Snik, J. H. H. Rietjens, A. Apituley, H. Volten, B. Mijling, A. Di Noia, S. Heikamp, R. C. Heinsbroek, O. P. Hasekamp, J. M. Smit, J. Vonk, D. M. Stam, G. Harten, J. Boer, and C. U. Keller, "Mapping atmospheric aerosols with a citizen science network of smartphone spectropolarimeters," Geophys. Res. Lett. **41**, 7351–7358 (2014).
31. G. van Harten, *Spectropolarimetry for planetary exploration*, (Leiden University Press, 2014).
32. G. van Harten, F. Snik, J. H. H. Rietjens, J. M. Smit, and C. U. Keller, "Spectral line polarimetry with a channeled polarimeter," Appl. Opt. **53**, 4187–4194 (2014).
33. C. Packham, M. Escuti, J. Ginn, C. Oh, I. Quijano, and G. Boreman, "Polarization gratings: a novel polarimetric component for astronomical instruments," Publ. Astron. Soc. Pac. **122**, 1471–1482 (2010).
34. C. U. Keller, "Design of a polarimeter for extrasolar planetary systems characterization," Proc. SPIE 62690T (2006).
35. M. Rodenhuis, H. Canovas, S. V. Jeffers, M. de Juan Ovelar, M. Min, L. Homs, and C. U. Keller,"The extreme polarimeter: design, performance, first results and upgrades," Proc. SPIE 84469I (2012).

1. Introduction

1.1. Multi-dimensional remote-sensing

When obtaining spectra of extended objects, we need to record light intensity as a function of image position and wavelength. This is challenging because it requires that three dimensions of information are captured on a detector that is generally 2D. This has led to the development of e.g. scanning slit spectrographs (in which one spatial direction is scanned in time), and integral-field units (in which the field of view is cropped into smaller sections, each of which is spectrally dispersed and imaged onto the detector using image slicers or fibers). For a review about the development of spectroscopy, see [1]. When measuring polarization or polarization-spectra, this problem is aggravated by the need to capture 2 additional quantities that describe the polarization state, which amounts to a 5-dimensional measurement. Therefore, imaging polarimeters or spectro-polarimeters generally require moving parts to scan through polarization directions or wavelength in time, or multiple beams, each with their own optics and detectors.

Optics EXPRESS

Implementations using moving-parts or multiple beams lead to non-common path errors, and are not always desirable when complexity needs to be low. In recent years, several novel design concepts have been proposed to overcome these limitations, to allow for instantaneous imaging spectroscopy (e.g. [2]), imaging-polarimetry (e.g. [3,4]) or imaging spectro-polarimetry (e.g. [5]). These devices exploit the wavelength-dependent properties of polarization optics to encode polarization information in the spectral dimension (i.e. spectral modulation, as first proposed by [6]), and collapse the remaining dimensions onto the detector plane using interferometric or tomographic methods.

Ref. [7] presents a spectral modulator that performs snapshot spectro-polarimetry and is optimized for measuring linear polarization. The intensity spectrum is modulated by a sinusoidal modulation that encodes for the linear polarization fraction and angle. In the current work, we present a new design concept that combines this spectral modulation with a micro-lens array. This results in a spectro-polarimetric integral-field unit that obtains the linear polarization spectrum of a grid of independent field-points, in a single exposure without moving parts.

We present this design in the context of an ongoing challenge in astronomy: The search for habitable planets around other stars and the signatures of extra-terrestrial life. However, polarization measurements are important in a wide range of fields, including medical, defense, surveillance, climate and environment, and we expect that this type of device can find many applications outside astronomy as well.

The scientific background is expanded upon in the remainder of this section. Section 2.3 explains the science requirements and the working principles of our design. Section 3 introduces a laboratory proof-of-concept, followed by a discussion of its performance in section 4. Finally, section 5 describes the steps that we still need to take to optimize this instrument for a real-world application as part of a space-mission.

1.2. Polarization of (exo)planets

Polarimetry is widely used in astronomical observations, for example to study the planets in our solar system, interstellar dust-grains, circumstellar material and the magnetic fields of stars (see [8,9] or [10] for comprehensive reviews). An enduring and important challenge in astronomy is the search for habitable planets that orbit other stars (extra-solar planets or 'exoplanets', in short). Much effort is directed at finding these exoplanets and studying their characteristics after having been discovered. The latter is especially problematic because planets are tiny compared to stars and they emit or reflect very little light compared to their host stars. The main challenge of exoplanet astronomy is thus to develop methods to increase the contrast between a star and its accompanying exoplanet. The fact that the contrast ratio (at visible wavelengths) between the brightness of the Sun and the Earth as seen by an interstellar observer amounts to 10^{-10}, shows that finding and studying an Earth-like exoplanet is a formidable challenge.

The light reflected by an exoplanet may be significantly polarized, depending on the scattering geometry (i.e. the illumination angle or 'phase' of the exoplanet) and the composition and structure of the planet's atmosphere and/or surface. This means that exoplanet observations may benefit from polarimetry. Firstly because the contrast between the bright star and the much fainter exoplanet is enhanced by filtering out the unpolarized starlight. Secondly, because the angle of linear polarization is determined by the on-sky position of the planet with respect to the star (position angle), a polarimeter filters all possible noise sources that emanate from directions other than the physical location of the planet. Thirdly, because the scattering, absorption and reflection properties of materials are wavelength-dependent, spectro-polarimetric information provides additional diagnostics of an exoplanet's atmosphere and surface [11, 12]. A good example of the use of polarization in planetary science is provided by [13], who used the polarization spectrum of Venus to determine that its upper cloud deck is composed of sulfuric acid. This could not have been derived from flux measurements of Venus. Also in the case of climate research, polarization

Optics EXPRESS

information is essential to determine the properties of the different types of aerosols in the Earth's atmosphere (see e.g. [14]).

As bigger telescopes and more advanced instruments are being constructed, the field of exoplanet research is focusing on establishing whether particular exoplanets satisfy minimal conditions for being habitable, and on the search for so-called 'biomarkers': observables that are uniquely indicative of extra-terrestrial life. An example of a biomarker is the spectral absorption band of molecular oxygen (O_2) between 759 and 770 nm. Molecular oxygen is regarded a biomarker because the presence of oxygen in the Earth's atmosphere is the result of organic photosynthesis. Photosynthesis causes the atmosphere to be in chemical *disequilibrium* and without a constant supply of oxygen from biological sources, the EarthâĂŹs atmospheric oxygen would be lost to chemical and surface reactions on time-scales of 10^6 years [15]. Oxygen absorption in the spectrum of an exoplanet therefore indirectly reveals the presence of extra-terrestrial organisms (though in certain cases, abiotic sources of oxygen may exist, see [16]). Vegetation also directly contributes to the reflection spectrum of an exoplanet. Chlorophyll -a family of biomolecules responsible for the absorption of sunlight in the process of photosynthesis- reflects sunlight at green wavelengths between 500 and 600 nm and in the near-infrared beyond 700 nm. These spectral features are called the 'green bump' and the 'red edge', are observable in the Earth's spectrum due to the planet-wide presence of photosynthetic organisms [17, 18]. It was shown by [19] that chlorophyll in photosynthetic microbes and plant-leaves induces circular polarization upon reflection. This is attributed to the fact that chlorophyll (like many other biological compounds) exhibit *homochirality*: The preferential occurrence of one particular configuration of an asymmetric molecule. It is believed that homochirality is a necessary attribute of the information-replicating processes which make life possible and it may even be a defining aspect of life itself [20]. Although multiple scattering of light by aerosol and cloud particles, and single scattering by some types of aerosol particles, are known to produce circular polarization as well, the spectral properties of homochiral biomatter are so distinctive that circular polarization can be concluded to be a powerful biomarker.

1.3. Earth as a model exoplanet

Future (polarization) observations of Earth-size exoplanets will necessarily be disk-integrated, because the spatial resolution of even the largest telescopes currently conceived is insufficient to resolve them. To assess the habitability of such planets, these observations will be compared to disk-integrated models of the Earth, which represent observations of Earth as if it was observed from far away. At the same time, we need to understand how different surface components contribute to the Earth's total polarization spectrum, so that a variety of distributions of Earth-like surface types can be matched to observations. To reliably retrieve habitability-indicators from future spectro-polarimetric data, versatile and well-tested benchmarks of the Earth must thus be available.

Ref. [21] calculated the Earth's disk-integrated polarization spectrum for different diurnal phases (i.e. with major landmasses, the pacific ocean or clouds dominating the spectrum); as well as the disk-integrated polarization strength as a function of illumination angle (phase). They confirm that the polarization spectrum provides an extra dimension along which to discern clouds from liquid oceans from landmasses - the latter two being especially difficult to discern by the shape of the disk-integrated spectrum alone. Another important prediction is the visibility of the polarization of the rainbow at $\sim 30°$, caused by high-altitude water droplets. As such, the polarization phase-curve can reveal the presence of water vapour, a very important ingredient of an Earth-like biosphere [12].

Attempts at measuring the Earth's polarization spectrum have been made before. One technique is to use Earth-shine: Sunlight that is reflected by the dayside of the Earth, onto the dark side of the Moon, into a telescope on the night-side of the Earth. Excitingly, Earthshine measurements have

Optics EXPRESS

revealed that the Earth's vegetation leaves strong biomarkers in the global reflection spectrum of Earth [22] and it might also leave a trace in the global polarization spectrum [23]. However, Earthshine suffers from a number of drawbacks:

- Any telescope can only see the Earth-shine coming from the hemisphere it is located on. That means that in order to measure the Earth's globally averaged polarization spectrum, Earth-shine observations need to be performed with telescopes spread out over the world. Measurements taken with various instruments under various circumstances would need to be combined, introducing systematic errors.
- Earthshine is observed on the un-illuminated side of the Moon. Therefore, the range of Earth's phase angles accessible to Earthshine observations is limited, because near full-Moon and new-Moon, Earthshine can never be observed.
- When Earth-shine is reflected off the lunar surface, it partly de-polarizes. This depolarization has a spectral dependence, varies across the lunar surface and is generally not well understood. The de-polarizing behaviour of the lunar surface can not be measured by mapping the polarization of sunlight reflected from the Moon. This is because polarization and de-polarization constitute different elements of the Mueller matrix. In the case of polarization, part of Stokes-I is transferred to Stokes-Q and U. However, in the case of de-polarization, part of Stokes-Q and U leak back into Stokes-I. See [24] for an attempt at taking lunar de-polarization into account.

Besides Earthshine, the POLDER and PARASOL instruments produced polarization maps of the Earth's surface in the context of climate science [25, 26]. These instruments however, are in low-Earth orbit and see only a small part of the Earth at any given instance of time. They therefore can't provide a measurement that integrates the light reflected off the entire planet in a single observation [27]. Also, these observations were exclusively broad-band, so only limited spectral information has been obtained from orbit.

A common orbit further away from Earth is geostationary orbit, 35,786km above the surface. From this distance, the Earth has an angular diameter of 21° and can be imaged in one frame. However, the instrument would always see the same hemisphere of Earth, per definition of geostationary orbit. There are currently no spectro-polarimeters in geostationary orbit, and to observe the Earth as if it would be an exoplanet, the instrument should be located still further away.

1.4. LOUPE: Spectropolarimetry from the lunar surface

[28] propose to observe the Earth with a space-based spectropolarimeter, using the lunar surface as a sufficiently distant platform to produce disk-integrated polarization spectra. The surface of the Moon provides a stable vantage point from which the Lunar Observatory for Unresolved Polarimetry of Earth (LOUPE) can observe the Earth at all times. The Moon is tidally locked to the Earth, which means that the same side of the Moon always faces the Earth, and from any point on the Earth-facing side of the Moon, the Earth is always at approximately the same position in the sky. The diurnal rotation of the Earth allows the entire Earth's surface to be observed every 24 hours, and all phase-angles are scanned during each lunar orbit.

From the lunar surface, the instrument will thus produce a full set of benchmark data after one month of observations, covering all configurations at which the Earth could be observed if it had been an exoplanet in an edge-on orbit (note that an exoplanet in an inclined orbit will show a limited range of phase angles). A lifetime in the order of a few years would additionally make these observations sensitive to the effect of seasonal variations.

Ref. [28] formulate conceptual requirements that these observations should minimally fulfil to produce the necessary scientific output, and propose four possible implementations of LOUPE to

Optics EXPRESS

accomplish this, either by measuring only linear polarization or the full Stokes vector; and with or without spatial resolution (i.e. imaging capability). In this paper, we present the development of a laboratory prototype of LOUPE that performs linear spectro-polarimetry with imaging capability. Although spatially resolved observations of exoplanets will not be possible in the foreseeable future, this implementation of LOUPE will allow the disk-integrated polarization spectrum to be obtained while simultaneously measuring local reflection properties. This information can be used to understand the individual contributions of the Earth's major surface features to the globally averaged polarization spectrum, and make the benchmark observations more flexible when applied to Earth-like exoplanets with different surface distributions. We constructed a proof-of-concept using off-the-shelf optics and demonstrate that the instrument can be small, robust, and fully solid-state; and we conclude that this instrument can be a valuable addition to any lunar mission without having a large impact to the resources and complexity of the payload.

2. Design of LOUPE

2.1. Science-derived instrumental requirements

An outline of the scientific requirements of LOUPE were listed by [28]. These are adapted and expanded below to illustrate the driving factors behind the design of our proof-of-concept for LOUPE.

1. Observations capture the entire disk of the Earth at any time.
2. Observations cover all diurnal phases and all phase angles of Earth. From the lunar surface, this translates to an instrument lifetime in excess of 1 month, with an observing frequency of more than once per hour to resolve the Earth's rotation.
3. Observations minimally cover known biomarker signatures in the optical part of the spectrum: The green bump between 500 – 600 nm, the vegetation red edge between 700 – 760 nm and the O_2A band between 750 – 770 nm.
4. The spectral resolution for polarimetry is 20 nm.
5. Considering that we wish to observe features at the level of the variations predicted by the polarization models of Earth as shown by [21], the fraction of linear polarization P_L is measured at every wavelength with a sensitivity in the order of 0.1% and an absolute accuracy of 1%.
6. The instrument leaves a small footprint on the resource budget of the lander vehicle, such as size, mass, power consumption, data transfer bandwidth. The quantification of such parameters is beyond the scope of this paper.

Although the Earth is always visible from any point on the Earth-facing side of the Moon, the non-zero eccentricity of the lunar orbit does cause the Earth *librate* over the course of the orbit, with a projected extent of $\pm 8°$. Assuming a low level of mechanical complexity of the LOUPE instrument, we discard active pointing of the instrument to track the motion of the Earth on sky. This means that a field of view of at least $\sim 20°$ by $\sim 20°$ is needed to have the Earth (which itself has a diameter of 2°) in view at all times. This field could be integrated as a whole, but only if the Earth is not close to the horizon, and when the Sun is not in the field-of-view (at phase-angles clouse to 180°). Given that the parameters of the lunar mission of which LOUPE will take part are not yet known (the lunar horizon would likely be in view on a mission to the lunar polar regions), and that we wish to observe the Earth's polarization spectrum also at large phase angles when the angular distance between the Earth and the Sun is small, leads us to develop a solution with imaging capability. This has the major benefit that spatial resolution

Optics EXPRESS

enables the independent characterization of the Earth's major surface features. By sampling the field of view with a grid of $\sim 50 \times 50$ spatial elements, the angular resolution of LOUPE is $\sim 0.4°$, equivalent to the angular scale of Earth's continents as seen from the Moon. For each such spatial point we then obtain a polarization spectrum, and any spatial point that sees the lunar horizon, the Sun or black space, will in principle not affect the measurement of Earth's disk.

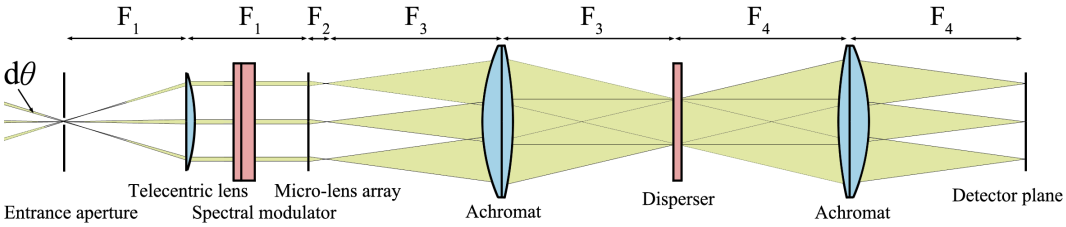

Fig. 1. Schematic layout of LOUPE. Light enters through the aperture on the left. The three different beams are three examples of the $N \times N$ beams generated by the MLA, each of which will see a slightly different direction on the sky. Spectral dispersion is not shown.

2.2. IFU design

Our design is shown schematically in Fig. 1. The field-of-view is determined by an entrance aperture in the focus of a telecentric lens. This aperture is small compared to the focal length F_1 of the lens, so all rays passing through the aperture exit the lens in parallel. The parallel beam then passes through the polarization modulation optics described in section 2.3 below.

To achieve imaging capability, we place a micro-lens array (MLA) at the back focus of the telecentric lens. An MLA is a two-dimensional grid of $N \times N$ lenslets, each of which sees a different part of the field of view and creates its own image of the entrance aperture a focal distance F_2 away from the array. The image plane of the MLA thus consists of a grid of $N \times N$ micro-images of the entrance aperture, referred to as *micro-apertures*. This grid of micro-apertures is subsequently imaged onto a detector using a pair of achromats with focal lengths F_3 and F_4 so the detector sees a grid of $N \times N$ images of the entrance pupil. The FOV is determined by F_1, the magnification of the field is determined by the ratio of F_3 and F_4, and the magnification of each micro-pupil is determined by the ratio of F_2 and F_3. We place a dispersion element in the middle of the $4f$ re-imaging system to spectrally disperse each of the $N \times N$ micro-pupils into a *micro-spectrum*.

2.3. Spectral polarization modulation

We use polarization modulation to simultaneously encode the intensity and polarization measurement along the wavelength axis of the spectrum. This can be accomplished by exploiting the strong wavelength-dependence of some polarization optics, which cause a sinusoidal intensity modulation to be imprinted on top of the intensity spectrum. The idea of encoding the full Stokes vector into the spectral dimension of a spectrograph was first described by [6] and [29]. [7] proposed to use a polarization modulator (sometimes referred to as a *channelled spectro-polarimeter* in the literature) that only measures the linear polarization spectrum, to detect and characterize the atmospheres of solar system planets. Since then, this scheme has also been used in iSPEX, a citizen science project aimed at measuring aerosols in the Earth's atmosphere using smartphones [30], and we use the same concept as the basis for our proposed implementation of LOUPE.

Polarization modulation works by stacking a $\frac{\lambda}{4}$-plate (QWP), a multiple-order retarder with retardance $\delta(\lambda)$ and a linear polarizer such that either axis of the QWP is aligned with the linear polarizer, while the axis of the multiple-order retarder is at a 45° angle with the other two. A

Optics EXPRESS

linearly polarized input spectrum $S_0(\lambda)$ will receive a modulation that is sinusoidal in frequency (see Eq. 1). The amplitude of the modulation scales with the polarization fraction P_L, while the phase scales with the polarization angle, ϕ_L. Both can be obtained by fitting a curve to the modulated spectrum [7].

$$S_{\pm}(\lambda) = \frac{1}{2} S_0(\lambda) \times \left[1 \pm P_L(\lambda) \cos\left(\frac{2\pi\delta(\lambda)}{\lambda} + 2\phi_L(\lambda)\right)\right] \tag{1}$$

Depending whether the linear polarizer is aligned with either the fast or the slow axis of the QWP, the modulation shifts by 180°. If both these channels are obtained, they can be added to yield the original intensity spectrum without the modulation. The modulation itself is recovered by subtracting the two channels and normalizing it with the intensity-spectrum:

$$S_+ + S_- = S_0(\lambda) \tag{2}$$

$$\frac{S_+ - S_-}{S_+ + S_-} = P_L(\lambda) \cos\left(\frac{2\pi\delta(\lambda)}{\lambda} + 2\pi\phi_L(\lambda)\right) \tag{3}$$

Light enters the polarization modulation optics through the entrance aperture and the telecentric lens, which together generate the desired field-of-view. As mentioned before, all rays passing through the aperture exit the lens and pass through the polarization modulation optics in parallel. This is important, because the retardance of waveplates depends on incident angle. Also, polarization-active optics should be as close to the front of the instrument as possible to reduce instrumental polarization induced by preceding optics. When exiting the polarization modulation optics, the beam continues to the MLA, where it is split up into micro-images of the aperture, each of which is then individually re-imaged and dispersed.

2.4. Optical configuration

The MLA can be rotated around its optical axis, such that the dispersion direction is at an angle α with respect to the micro-pupil grid (see Fig. 2). A proper choice of α stacks the micro-spectra onto the detector in such a way that cross-talk between adjacent spectra is minimized, while maximizing the number of detector pixels that can be used effectively. The optimal choice for α depends on the length, width and number of micro-spectra. This means that there is trade-off between spectral range, spectral resolution, spatial resolution, field of view and light-gathering power. The available detector pixels have to be divided over the $N \times N$ micro-spectra, so a higher spatial resolution (larger value of N) or a larger field-of-view necessarily decrease the spectral performance. Conversely, a larger spectral range and higher spectral resolution require the spectra to be dispersed over a larger number of detector pixels, limiting the value of N for a given detector size. Similarly, if the light-gathering power is increased by increasing the entrance aperture, the width of the resulting micro-spectra increases accordingly, requiring a larger value for α, and thus shorter micro-spectra (less spectral bandwidth or dispersion). This trade-off allows for great flexibility in the application of this design. Depending on the application, a direct exchange between spatial and spectral range and resolution and light gathering power can be made, using only robust steady-state components.

We conservatively assume that the grid of micro-spectra should fit on a 1k by 1k detector because larger detectors are rare in space-based applications. This upper limit on the amount of pixels, limits the information density of the observations and the implementation of LOUPE should thus focus on de-magnifying and re-imaging the entrance aperture as finely as possible to allow for optimal stacking of the micro-spectra onto the detector. In the case of LOUPE, light gathering power is not a major issue because the Earth is a bright target, so LOUPE will use a small entrance aperture. Therefore, the imaging performance of the instrument determines the point-spread-function of the micro-apertures which then constrains the physical pixel size of

Optics EXPRESS

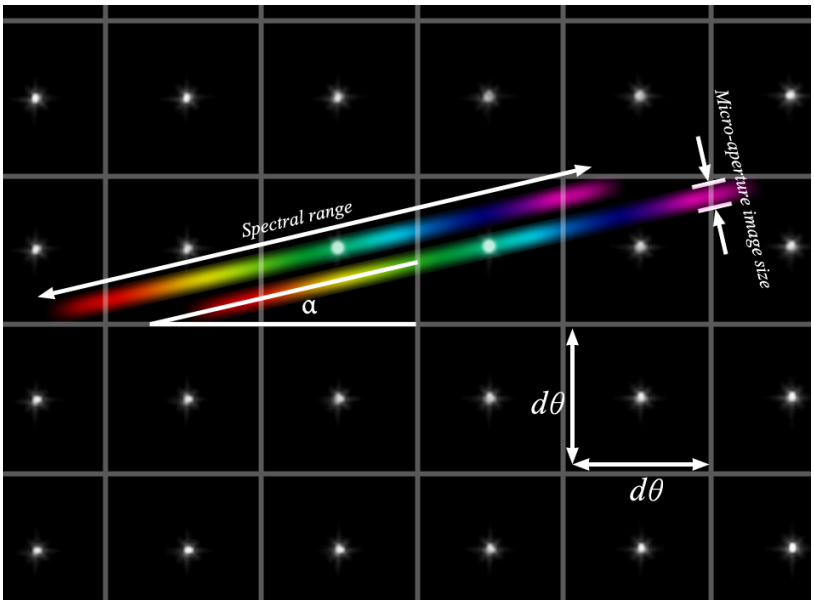

Fig. 2. A read-out of the grid of micro-apertures, overlaid with a schematic illustration of how micro-spectra are stacked to fill the detector array. By rotating the grid of micro-lenses by an angle α with respect to the spectral dispersion direction, the micro-spectra can be stacked side-by-side. The smaller α can be made without lateral overlap, the more space there is in the dispersion direction for an increase in bandwidth or spectral resolution. The width of the spectra is determined by the magnification of the micro-apertures onto the detector, or the point-spread function of the re-imaging achromats, whichever dominates. The suppression of aberrations is therefore crucial to stack the micro-spectra efficiently.

the detector: If the pixel scale of the detector does not match the point-spread-function of the micro-aperture, the image of the micro-spectrum on the detector will be under or oversampled.

If the grid of micro-spectra measures 50×50 elements, a total of 2500 micro-spectra should be contained in a single image. In order to fully obtain the polarization modulation, each micro-spectrum should be imaged in two polarization channels simultaneously (see section 2.3). Therefore there are 200 pixels per individual micro-spectrum available on a 1k×1k detector. If we further assume a bandwidth of 250nm, a PSF measuring 2 pixels, and a margin of 1 pixel around all sides (to prevent lateral cross-talk between micro-spectra), the dimensions of a micro-spectrum are 50×4 pixels, which results in a pixel scale of 5.0nm/px and a spectral resolution of 10nm/px. This is enough to sample a polarization modulation with a period of 20nm as dictated to be a requirement in section 2.1. This pixel budget is thus theoretically sufficient to satisfy the sampling requirements. However, stacking the micro-spectra onto the detector is a serious challenge. This is why our proof-of-concept will be limited to the single-beam implementation of the polarization modulation scheme, and we note that the pixel budget can be relaxed greatly by choosing a larger detector (see Section 5).

3. Proof of concept

3.1. Optics

From left to right in Fig. 1 we have chosen the following optical components: The entrance aperture is a circular pinhole with a diameter of 1 mm. It is placed in the front-focus of a plano-convex $F_1 = 150.5$ mm lens with a diameter of 25.4 mm, made of fused silica to minimize

Optics EXPRESS

stress birefringence. At the back focus of this lens, we place a square, 68 × 68 MLA measuring 15 × 15 × 1mm^3, with a focal length of 0.93 mm. The polarization modulation optics is placed between the lens and the MLA, and consists of a zero-order QWP, a stack of six 4λ retarding polymer films (the same films are used in iSPEX [30]) and a 2" linear polarizer. The linear polarizer needs to be rotated to obtain the two complementary polarization channels sequentially. It is therefore placed in a rotation mount, so that it can be aligned to either axis of the QWP (see Section 2.3) This implementation therefore does not perform *snapshot* imaging polarimetry, as a sequence of two exposures is needed to capture both polarization channels. In Section 5 we discuss how this will be addressed in future iterations.

The focal plane of the MLA is re-imaged by a pair of identical 2" achromats with a focal length of 100 mm, spaced 200 mm apart. The dispersive element is a right-angle N-BK7 prism placed on a rotation platform in the middle between the re-imaging lenses. Because the spectral dispersion depends on the incident angle of the beam onto the prism, the dispersion can be fine-tuned by rotating this platform. The advantage of using a prism is that the dispersion increases towards blue wavelengths. This counters the decrease in the fast periodicity of the modulation at blue wavelengths, which scales with $\frac{1}{\lambda^2}$ [7].

At the image plane is a Point Grey Flea3 1.2 megapixel monochromatic CMOS camera. The detector consists of 1280 × 1024 square pixels, measuring 5.3 μm × 5.3 μm, and thus spans a total area of 6.8 × 5.4 mm^2. The detector is aligned to the dispersion direction of the prism, so that the micro-spectra are imaged horizontally on the detector. Because the magnification of the two achromats is unity, the image plane of the MLA matches the size of the MLA itself, which has an effective diameter of 14 mm. Therefore, this detector sees only a quarter of the re-imaged micro-pupils, and thus covers only a quarter of the total FOV. The micro-spectra are dispersed in the direction of the long side of the detector, and the micro-pupil grid is rotated such that the spectra do not overlap, and cross-talk between adjacent micro-spectra due to the wings of the PSF, is minimal (see Fig. 2 and Section 2.2). In order to reduce aberrations induced by the re-imaging lenses, we add a circular field stop and an 800 nm short-pass filter behind the first achromat. Regardless, because the pixel scale of 5.3 μm^2 is small, the spectral performance of this implementation will be limited by the imaging performance of the optics, as the spectral resolution is limited by the point-spread-function of the micro-apertures, rather than the spatial sampling of the detector array. This oversampling of the PSF is not relevant for our demonstration of the working principle of LOUPE.

The F_1 = 150.5 mm objective lens generates a circular FOV with a diameter of 9.6°. The beam exiting the lens has a diameter of 25.4 mm, which is subsequently vignetted by the mount of the MLA which has a circular clear area 14 mm wide. This thus cuts the total FOV to a diameter of 5.3°. Although this is much smaller than the required 20° FOV, we note that the FOV can be increased trivially by reducing the focal length of the lens to ~ 40 mm. However, we chose a slower lens because 4 cm between the lens and the MLA would have been insufficient to fit our polarization modulation optics. The image plane of the MLA is re-imaged onto the detector with unity magnification, so the grid of micro-spectra is circular with a diameter of 14 mm. The detector measures 6.8 × 5.4 mm^2, so it sees only a quarter of the re-imaged micro-pupils, and thus covers only a quarter of the already vignetted FOV. This can be mitigated by choosing a detector with larger pixels.

3.2. Test observations

We have simulated science spectra with our LOUPE prototype using a Styrofoam sphere as a model planet. The sphere (with a diameter of 7.8 cm) was illuminated by a slide projector at an angle of $10° < \gamma < 90°$ with the line of sight to the instrument, which was located at a distance of ~ 3 meters from the target. Observations consist of median-combined sequences of ten 1ms exposures to reduce photon-noise. In each polarization channel (Eq. 3), we also obtain such a

Optics EXPRESS

sequence of wavelength calibration frames, polarization calibration frames and dark frames.

To assess how the prototype performs at retrieving the polarization of the Styrofoam target, we obtain control-measurements using a standard imaging-polarimetry setup: The target is imaged onto the camera by a single lens that is preceded by a linear polarizer. We obtain the image at visible wavelengths (between 400 nm and 800 nm) in a horizontal (S_+) and a vertical (S_-) channel, parallel respectively perpendicular to the plane in which the light is reflected off the target. P_L is obtained by aligning and combining the two channels.

3.3. Data reduction

The detector images the grid of micro-spectra and saves them in 16-bit monochromatic TIFF images. We start the analysis by feeding a broadband deuterium-halogen lamp into the setup using a fiber, thereby uniformly illuminating the entrance aperture. This reveals each micro-spectrum at high contrast and allows us to establish the location and extent of all micro-spectra. The micro-spectra are surrounded by background flux, caused by aberrations, diffraction, internal reflections and other instrumental imperfections. In the uniformly illuminated image, we designate a collection of pixels between micro-spectra that are furthest away from the bulk of the flux of the surrounding micro-spectra. We fit a 3^{rd} degree polynomial surface to all these pixels in the image to get a measure of the background flux, which we subtract. Bad pixels are removed by interpolating pixel values that are more than 4σ away from their surroundings. Finally, the micro-spectra are cropped-out along rectangular areas, and extracted by adding the pixel rows of the cropped region. We co-add the rows with Gaussian weights, to weigh down rows away from the central pixel row, that are more sensitive to cross-talk from PSF-wings of neighbouring micro-spectra (see Section 4 for an analysis of the cross-talk in this setup). After extraction, we have thus obtained a 1D representation of each micro-spectrum.

3.4. Wavelength calibration

To obtain a wavelength calibration, we illuminate the entrance aperture with a HgAr line-lamp that emits 15 lines in the range between 450 to 820nm. We locate these lines in each micro-spectrum by obtaining the center-of-mass of each line and matching those to the known line-positions of the mercury-argon spectrum. Not all lines are resolved by LOUPE, so we match the center-of-mass of a group of unresolved lines to the center-of-mass of the known wavelength-positions, while weighing for the individual line strengths. We map pixel positions to wavelength by performing a 4^{th} degree polynomial fit, also weighted to the known line strengths. This yields a wavelength-solution for each extracted micro-spectrum.

3.5. Polarization calibration

The modulation as described by Eq. 3 scales with $P_L(\lambda)$ between 0 and 1. However in practise, our prototype is not able to produce a modulation with an amplitude of 1 when illuminated with fully polarized light. This is because the performance of the polarization optics is not perfect and wavelength dependent. Though the wavelength dependence of the multiple-order retarder was exploited to produce the polarization modulation, similar wavelength dependence of the QWP and the linear polarizer results in reduced efficiency at wavelengths away from the rated optimum wavelength of the optics. Similarly, the imaging performance of the lenses deteriorates near the edges of the wavelength range. This means that spectral resolution of the instrument decreases accordingly so that light from a maximum of the modulation may leak into the surrounding minima, decreasing the observed amplitude of the polarization modulation. This effect is especially relevant towards blue wavelengths, because the frequency of the polarization modulation increases with decreasing wavelength [7].

The wavelength-dependence of the efficiency of the instrument is calibrated by fully polarizing the deuterium-halogen input (see Section 3.3) using a linear polarizer. In our case, only a single

Optics EXPRESS

reflection geometry is relevant (see Section 3.2). Ideally however, we would calibrate Stokes-Q and U independently because the retardance of the QWP is not exactly $\frac{1}{4}\lambda$, which reduces the ability of the polarization modulator to register polarization in the direction of U [7, 31].

The calibration spectrum also yields a measurement of the retardance $\delta(\lambda)$ of the multiple-order retarder and the zero-point angle of the input polarization ϕ_L. These are represented by the frequency and the phase of the modulation, and are obtained by fitting the modulation (Eq. 3) to each calibration spectrum.

3.6. Demodulation

Equation 3 assumes that the transmission in both polarization channels is identical, in which case the modulation function oscillates around 0. However in practise, the throughput of the instrument will be slightly dependent on the input polarization, which means that both channels need to be normalized independently. We adopt the procedure outlined by [32], who iteratively correct the wavelength-dependent transmission for each channel $t_{\pm}(\lambda)$ by requiring that the integral over any period of the modulation is 0. The deviation from 0 is measured for $\sim$ 200 steps in phase (i.e. wavelength), which is then fit with a 4^{th} degree polynomial to obtain the wavelength-dependent transmission correction on $t_{\pm}(\lambda)$ (see Fig. 3).

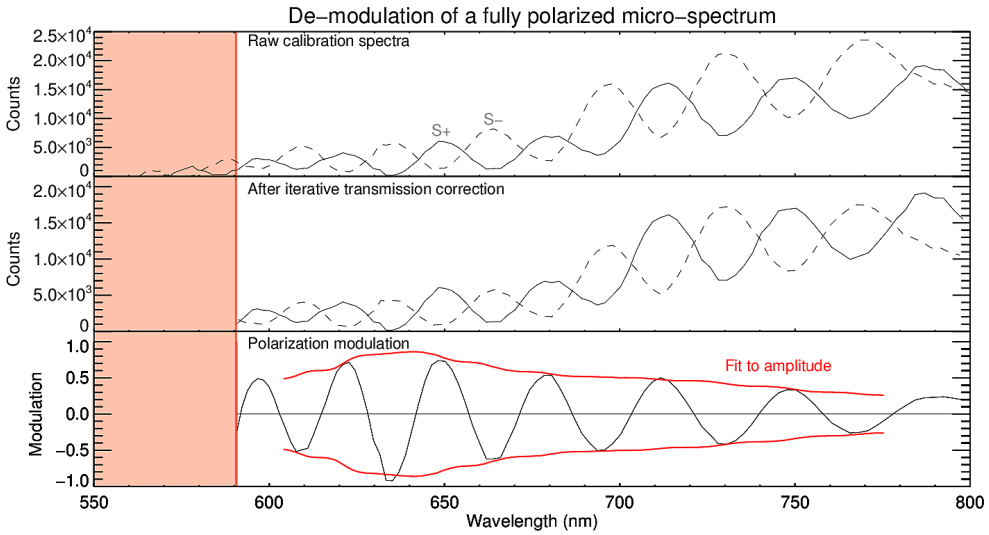

Fig. 3. Step-wise reduction of a single micro-spectrum from the two calibration channels (i.e. fully polarized input either in the horizontal or vertical direction). The top panel shows both channels of a single micro-spectrum after dark subtraction, background correction and extraction. In the middle panel, the two have been modulated such that the transmission in both channels is equalized. The bottom panel shows the extracted polarization modulations as described by Eq. 3. In order to obtain a polarization measurement from these, we fit the modulation (Eq. 3) to a ±15 nm range around each point. The measured amplitudes are then divided by the modulation amplitudes of the respective (fully polarized) calibration micro-spectra, the result of which yields P_L for each point. Note that the wavelength range is cut during the analysis. On the one hand, this is because of low signal-to-noise of the calibration spectra. On the other, chromatic aberrations deteriorate the spectral resolution towards shorter wavelengths, causing the polarization modulation to become unresolved. Also note that the efficiency of the spectral polarization modulation-optics at producing the polarization modulation (amplitude of the modulation), diminishes long-ward of 700 nm. This is due to the break-down of the linear polarizer at red wavelengths.

Optics EXPRESS

The corrected modulation is fit within bins of 20px (on average ~ 30nm) wide between wavelengths of 610 and 800 nm (as the efficiency of the modulation diminishes blueward of 610 nm), while keeping the retardance $\delta(\lambda)$ fixed to the value as measured by fitting the entire calibration spectrum. This provides a measurement of the average amplitude of the modulation per wavelength-bin, for both the "science" micro-spectra as well as their associated calibration micro-spectra (see Fig. 3). These are divided to yield the polarization spectrum of each field-point. The angle of polarization is obtained by subtracting the measured phases of the calibration spectra from those of the "science" spectra.

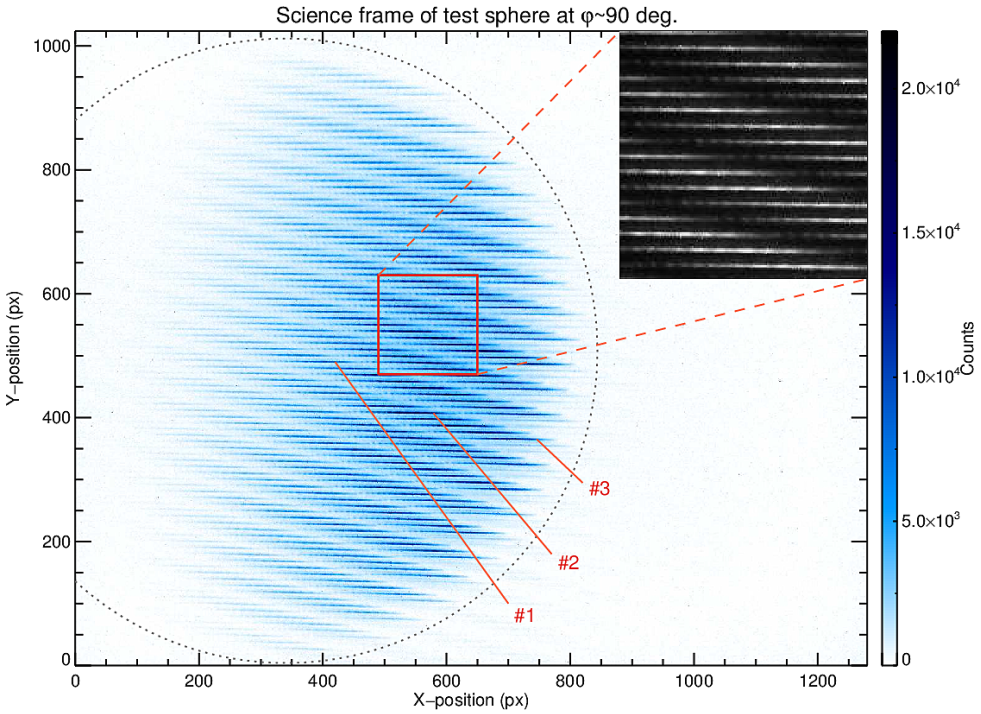

Fig. 4. A readout of a single LOUPE exposure while observing the Styrofoam test-sphere, illuminated to simulate a planet at close to 90° phase. Microspectra #1 to 3 are separately shown in figure 5, for illustrative purposes. Significant linear polarization is caused in this scattering configuration as evidenced by the fact that the polarization modulation can be observed by eye in the zoomed-in section in the upper-right.

4. Performance of the LOUPE prototype

Figure 4 shows a readout of the prototype, with the polarization modulations of three micro-spectra illustrated in Fig. 5, along with the resulting measurements of $P_L(\lambda)$. Each point of P_L is obtained by fitting the modulation curve in a range of ±15 pixels from that point, and therefore represents a ~ 23 − 42 nm bin (at 610 and 800nm respectively) within which P_L is measured. These measurements are subsequently smoothed to the bin-size [7], producing bin-averaged measurements of P_L with a typical scatter of a few %. This level of noise scatter is fully accounted for by photon noise in the micro-spectra (primarily noise in the science-frames because flux levels are low), readout noise and photon-noise in the background that was subtracted.

With a measurement of P_L for each micro-spectrum, we re-construct the spatial dependence of the polarization fraction across the image, and compare it with control measurements obtained with the linear polarimetry setup (see Section 3.2). Figure 6 shows this comparison for the

Optics EXPRESS

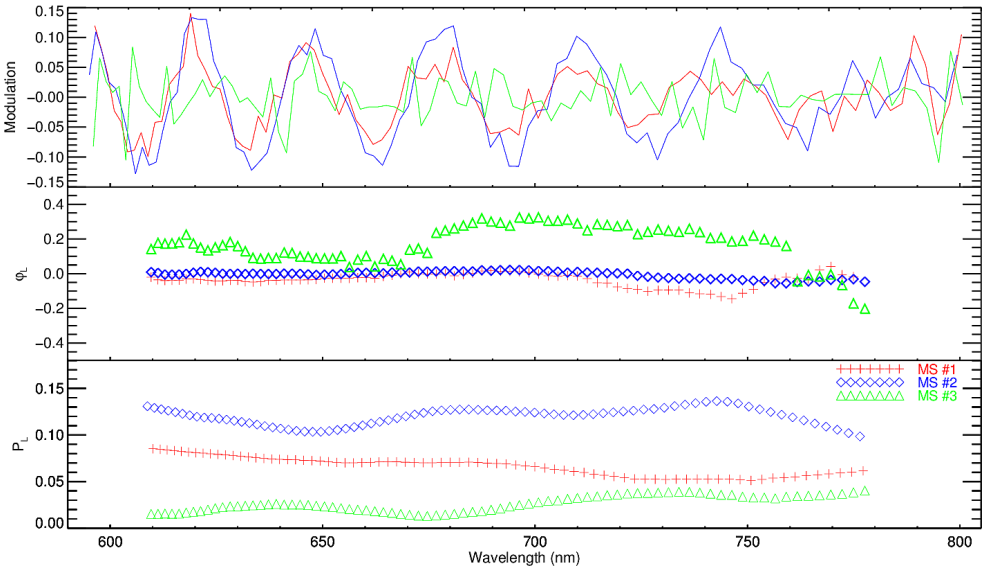

Fig. 5. Top panel: The three micro-spectra selected in figure 4 after extraction, wavelength calibration and transmission correction. Middle panel: The angle of polarization ϕ_L relative to the phase of the calibration spectra. The increased scatter in retrieved polarization angle of micro-spectrum #3 is reminiscent of the fact that the modulation is dominated by noise because the amplitude is low. Bottom panel: P_L is obtained by combining the two polarization channels of each according to Eq. 3 (only one channel is shown in the top panel), fitting the amplitude as a function of wavelength, and dividing the measured amplitudes by the corresponding amplitudes measured in the fully-polarized calibration micro-spectrum. Note that the wavelength-range is reduced at the edges, because the fit at the edge of the spectrum generates a measurement of P_L at the center of the fitting range, and that the measurement of P_L is smoothed with a box-window that matches the size of the fitting range around each point.

intensity images (top panels) and polarization (bottom panels). LOUPE is able to retrieve the major features in the polarization map, notably the specular reflection and decreasing polarization towards the edge on the right side of the sphere. Quantitatively, systematic errors clearly persist on the percent level: LOUPE seems to overestimate the polarization by a few percent near the edges of the disk, while not reproducing the strong polarization towards the poles observed in the control measurement.

There are a number of possible causes for systematic errors. Most importantly, there is the possibility that micro-spectra are stacked too closely together, causing cross-talk between neighbouring micro-spectra. Cross-talk is especially important when the amplitude of the polarization modulation is high (as is the case for the polarization calibration spectra) because the maximum of the polarization modulation of one micro-spectrum can strongly contaminate the minimum of an adjacent spectrum. This means that cross-talk is expected to peak at certain wavelengths [31]. For each pixel (in the spectral direction between 600 to 800nm, which covers all of our effective wavelength range, see Section 3.6) of each micro-spectrum, we modelled the integrated flux originating from all adjacent micro-spectra by fitting their lateral profiles with Gaussian distributions. We define cross-talk in any pixel, as the ratio of the flux originating from all neighbouring micro-spectra, to the total flux in the pixel. We find that for the micro-spectra onto which the Styrofoam sphere is imaged, the peak cross-talk exceeds 5% in three of the polarization calibration spectra, but never exceeds 5% in the science-frames. At the same time, the wavelength-averaged

Optics EXPRESS

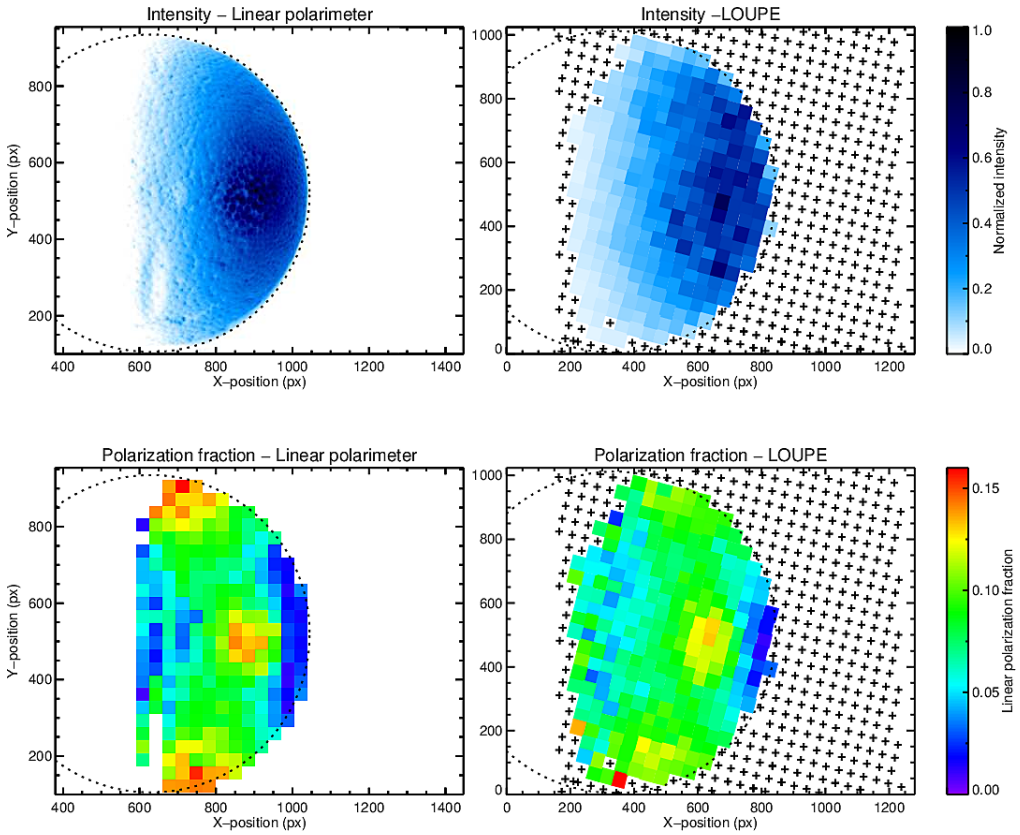

Fig. 6. Comparison of a measurement obtained by LOUPE versus a higher resolution image obtained using a standard linear polarizer. The target is the Styrophome sphere, illuminated from a right angle. The top panels show the raw intensity image of the linear polarimeter (upper-left, arbitrary colour scale), and the average of the intensity in the micro-spectra between 600 and 700nm, as determined for each micro-spectrum obtained by LOUPE (upper-right). The bottom panels show the resulting distribution of P_L on the sphere as measured by subtracting the two channels taken with linear polarimeter (bottom-left), and the average of P_L measured by LOUPE, also between 600 and 700nm (bottom-right). The control measurement of P_L in the bottom-left panel was blurred and down-sampled to the same angular resolution and grid-size as the measurement by LOUPE in the bottom-right panel. The colour scale is the same for both lower panels, which shows that LOUPE is able to reproduce the global variations in P_L, at the same qualitative level. The crosses in the right panels denote the locations of micro-spectra. This grid is slanted because the MLA is rotated with respect to the detector array. Only micro-spectra with sufficient flux were extracted and analysed.

cross-talk is never higher than 0.5% for any of the polarization calibration spectra, and never exceeds 0.2% for any of the science-spectra.

However, close examination of the high-contrast images used to calibrate the locations of the micro-spectra (Section 3.3) reveal the presence of a significant ghost associated with each micro-spectrum, caused by an internal reflection in the re-imaging system. These ghosts partly overlap with the cores adjacent micro-spectra and may cause significant cross-talk - as they can be discerned by eye. We therefore conclude that although cross-talk from the PSF-wings of adjacent micro-spectra cannot account for systematic errors of several percent on the measured

Optics EXPRESS

polarization levels, it is possible that an internal reflection can.

Besides cross-talk, there are a number of other sources of error that could contribute to the observed systematic variations, and which must also be addressed in future iterations. Firstly, the linear polarizer used to calibrate LOUPE, as well as the polarizer used in the imaging polarimeter with which we perform the control measurements, are wavelength-dependent and not calibrated. Similarly, the light-source used to illuminate the Styrofoam sphere is not stabilized and may be varyingly polarized.

Secondly, we have not characterized the instrumental polarization. The polarization-modulation optics are preceded only by a single objective lens which is made of fused-silica to minimize stress-birefringence. Although we expect this lens not to cause significant polarization, it was not calibrated for.

Thirdly, an incorrect extraction of large-scale background flux (the measurement of which is affected by the presence of ghosts) will offset all micro-spectra, decreasing the amplitude of the polarization modulation [7,31]. Fractionally, this would affect the polarization calibration spectra more strongly than the science spectra, causing an apparent excess of the derived polarization which will be dependent on the location in the field.

Fourthly, detector non-linearity was not characterized, and would again mainly affect the polarization calibration because the flux levels in these spectra were generally high.

Finally, because S_+ and S_- are obtained separately by manually rotating the linear polarizer of the polarization modulation optics, the two channels are not imaged on the same detector position, which introduces errors due to flat-field and defocussing.

We note that systematic errors on the percent-level are not unexpected, given the usage of rotating polarizers and an un-stabilized lightsource to perform calibration measurements. Solving these systematic errors by using better calibration data and by addressing the issues mentioned above with a more sophisticated data reduction method and higher quality components, is beyond the scope of this proof-of-concept. More importantly, there are some qualitative departures from the requirements stated in Section 2.1 and the design concept described in Section 2.2. These represent no fundamental barriers however, and possible avenues and considerations for addressing these issues in future iterations are discussed in the following section.

5. Optimizing the prototype model

5.1. Beamsplitter

The notion of a snapshot linear polarimeter is defeated when the polarization channels S_+ and S_- need to be obtained in sequence with a rotating polarizer, as is the case with this proof-of-concept. It uses a single beam setup whereas LOUPE should measure two beams simultaneously to do full linear spectro-polarimetry using snapshot observations. Dual-beam capability is achieved by replacing the linear polarizer with a polarizing beamsplitter. This doubles the density of micro-spectra on the detector array as noted in Section 2.3. We performed a trade-off analysis between a Wollaston prism, a Savart plate and a polarization grating.

- The Wollaston prism would be placed in the pupil-plane near the dispersive element. The two polarization channels exit the prism in diverging beams, with separation angle γ. The plane of separation is perpendicular to the dispersion direction of the dispersion element, such that the micro-spectra belonging to each channel are stacked laterally.

- The Savart plate is similar to the Wollaston prism, but would be placed in the focal plane of the MLA. It splits the two polarization channels into beams that exit the plate in parallel, with spatial separation d. The plane in which the beams are separated is again perpendicular to the dispersion direction, causing the micro-spectra to be duplicated in the lateral direction.

Optics EXPRESS

- The polarization grating would combine the functionality of a beamspltiter and a dispersion element [33], and be placed in the foci of the two re-imaging achromats. The polarization grating disperses the beam into two spectral orders, each in orthogonal polarization directions. The two orders lie on opposite sides of an undispersed zero-th order which serves as a direct measurement of the total integrated flux (Stokes-I).

Of these, we consider the Savart plate to be the best option for LOUPE. The advantage of the Savart plate over the Wollaston prism is that the separation angle of the Wollaston prism varies over the field, because the beams coming from the MLA pass through the prism at different incidence angles. The Savart plate does not have this problem because it is located in a parallel beam. An additional disadvantage of using a Wollaston prism, is that it would be sensitive to systematic polarization originating in the MLA and the first achromat. In contrast, the Savart plate is located one step earlier in the optical path. Finally, the separation between the exiting beams of the Savart plate depends on the thickness of the plate. To efficiently stack the micro-spectra the separation must be made small, which can be achieved by choosing a thin plate. By putting an achromatic half-wave plate (HWP) between the two parts of the Savart plate, any crystal abberations (primarily astigmatism) will be identical in both polarization directions which means that they can be corrected for using a cylindrical lens [34].

We favor the Savart plate over the polarization grating because in the latter implementation, optimally stacking the spectra onto a small detector is more complicated. With a polarization grating, the spectral dispersion and polarization splitting occur in the same direction. Ideally, spectra are stacked such that the gap between the zero-th and first order of one spectrum is filled by the first order of a nearby micro-spectrum [35]. This reduces the stacking efficiency at the edges of the field, where gaps between the dispersion orders will not be filled. For higher dispersion strengths, the orders will be further apart, so the total stacking efficiency will decrease with spectral resolution. In the case of the Savart plate, the spectral dispersion is decoupled from the polarization separation, allowing for more efficient stacking on a small detector.

5.2. Stacking

Figure 2 shows how single-channel observations are stacked onto the detector using the Savart plate. The lateral distance between micro-spectra in the single-beam setup is ~ 50 μm (10px, see figure 4) and if we assume the same margin in the dual-beam implementation, the length of each micro-spectrum should be halved in order to double the available space needed to image the second channel. Now the trade-off described in Section 2.2 is particularly relevant: Reducing the spectral dispersion reduces the bandwidth and/or the spectral resolution, provided that the detector pixels are shrunk accordingly. This has implications for the dimensions of the detector and the accessible field-of-view. Conversely, maintaining bandwidth and spectral resolution means that a smaller amount of micro-spectra can be fit onto the detector, resulting in a reduced spatial resolution or increased cross-talk, if spectra are to be stacked more closely to each-other.

We made a MATLAB simulation to optimize dual-channel stacking on a 1k by 1k detector considering the application of both a hexagonal and a square MLA. We assume square pixels with a size of 10×10 μm^2 and micro-spectra with a length of 64 pixels (slightly longer than theorized in Section 2.2), a width of 2 pixels and a lateral margin of 3 pixels (giving a total lateral distance of 5×10 μm $= 50$ μm between spectra). As argued before, better spectral characteristics can be achieved by reducing aberrations (which decreases the margin needed between adjacent micro-spectra) and by increasing the resolution and size of the detector array. From the MATLAB simulation it was found that optimal stacking with a hexagonal MLA occurs at a rotation angle of $\alpha = 12.5°$, in which case a maximum of 44×35 spectra can be fully imaged on the detector. In contrast, a square MLA allows a maximum of 32×34 spectra at a rotation angle of $\alpha = 26.5°$ (see Fig. 7). A hexagonal MLA therefore provides better stacking efficiency than a square MLA, which serves to show that the choise of micro-lens configuration is important

Optics EXPRESS

when designing an IFU using an MLA.

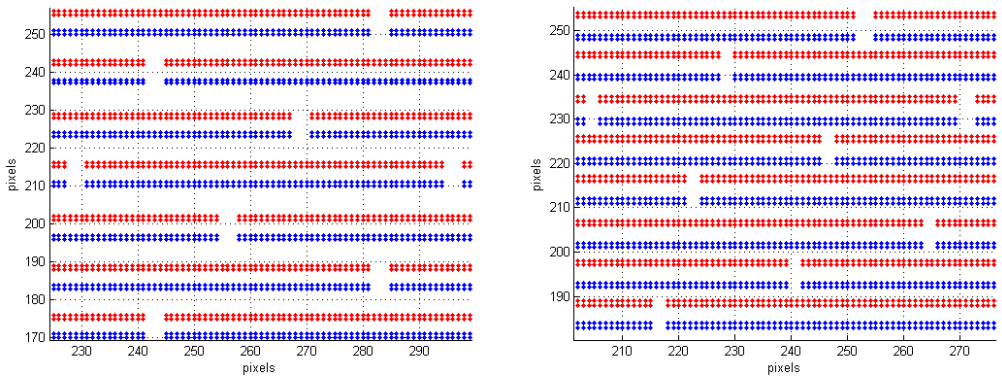

Fig. 7. Stacking using a square MLA (left), compared to a hexagonal MLA (right). The red and blue spectra denote the two polarization channels. For mictro-spectra with these dimensions, a hexagonal MLA grid allows for more efficient stacking than a square MLA grid.

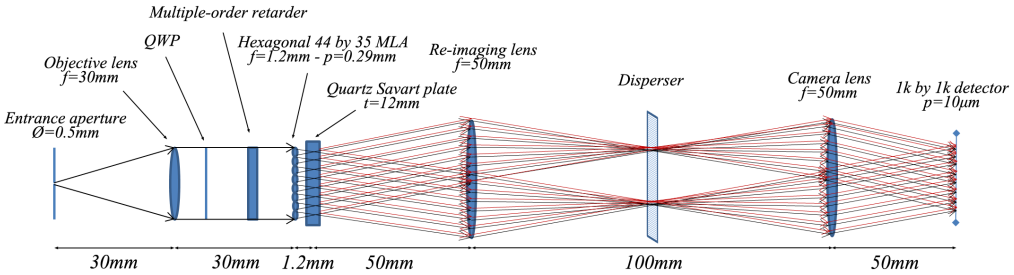

Fig. 8. The dual beam concept for LOUPE. The red and black beams emerging from the Savart plate represent the two orthogonal polarization channels. Dispersion is not shown.

5.3. *Proposed design implementation and further considerations*

Our proposal for the dual beam concept for LOUPE is shown in Fig. 8. The system has a one-to-one re-imaging pair behind the MLA with focal lengths of $f = 50$ mm. The hexagonal MLA contains 44×35 lenslets with a focal length of $f_{MLA} = 1.2$ mm and a lens diameter of 290 μm. To obtain a field of view with of 20°, the field lens should have a focal length of $f = 30$ mm, giving an $f/4$ system and a spatial resolution of 0.6° (3×3 samples over the Earth's disk). The image of the 0.5 mm entrance aperture will then have a diameter of 20 μm, corresponding to 2×2 pixels on a detector with 10 μm pixels. To achieve a lateral distance of 5 pixels between the spectra of the two channels, the Savart plate needs to be made of 12 mm thick quartz. As follows from Fig. 8, the dimensions of this design are approximately $26\times2\times2$ cm, which can be further compressed by folding the optical path, possibly using a Littrow configuration and if necessary, a three-mirror anastigmat.

In this design, micro-spectra have a length of 64px and a PSF size of 2 pixels, which can provide 32 independent spectral measurements between $500 - 800$ nm, equivalent to a spectral resolution of 9 nm, enough to sample a polarization modulation with a period of 20 nm, in line with the science requirements stated in Section 2.1. We do stress that an increase of the detector

Optics EXPRESS

size beyond 1k × 1k as well as a reduction of the spot size, would directly result in better spectral and spatial performance of this design.

Further issues that need to be addressed are the shielding of the instrument against extreme fluxes when the Sun is in view, the calibration of the instrument (either before the start of the mission or by adding the capability to calibrate the instrument after launch), the possibility of active-pointing (which would radically relax the field-of-view requirements and improve performance, but would involve moving parts which would increase the risk of failure), the (thermo-)mechanical and electrical design, power (power usage will be low owing to the solid-state design) and data handling (considering the possibility of on-board processing).

6. Conclusion

This paper presents a proof-of-concept for the Lunar Observatory for Unresolved spectro-Polarimetry of Earth (LOUPE). From the Earth-facing side of the Moon, LOUPE will measure the polarization spectrum of Earth over all phase-angles and diurnal phases, to generate a benchmark for future polarization observations of exoplanets, as initially proposed by [28]. Such benchmarks are needed to verify the polarization models that will be used to infer physical characteristics of the exoplanet environment from their polarization spectra and phase-curves, and to optimize instrumentation for direct observations. The design we propose is the first snapshot spectro-polarimetric integral-field unit: A linear spectro-polarimeter with spatial resolution. This is accomplished using a robust solid state design without moving parts and the polarization modulation principle in combination with a micro-lens array.

We constructed a prototype using off-the-shelf components, and prove that this design for LOUPE is able to retrieve spatially resolved spectro-polarimetric observations of a mock planet target. These observations are affected by systematics on the percent level, which we mainly attributed to a combination of ghost images and instrumental polarization caused by the optics and the light-source. The main shortcoming of our proof-of-concept is that it relies on a rotating linear polarizer to obtain both polarization channels S_+ and S_- in sequence. However, we have discussed the most important avenues for solving this shortcoming by incorporating dual-beam functionality using a Savart plate, and modelled how the micro-spectra can optimally be stacked onto the detector using a hexagonal micro-lens array. Finally, we have identified the issues that remain to be addressed to reach a fully capable flight-model.

Due to its low level of complexity and small size, this design is ideal for application in space, and we are in the process of designing a flight-model for LOUPE. In addition, we note that the flexibility in its optical and spectral characteristics allow applying our design to a wide range of problems in which spatially resolved spectro-polarimetry is required.

Funding

Netherlands Organisation for Scientific Research (NWO); Project 639.043.503.